Shell evolution and isomers below ^{132}Sn: Spectroscopy of neutron-rich $_{46}$Pd and $_{47}$Ag isotopes

Hiroshi Watanabe[1,2,*]

[1]IRCNPC, School of Physics and Nuclear Energy Engineering, Beihang University, Beijing 100191 China
[2]RIKEN Nishina Center, 2-1 Hirosawa, Wako, Saitama 351-0198, Japan

Abstract. Neutron-rich isotopes of Pd ($Z = 46$) and Ag ($Z = 47$) have attracted considerable interest in terms of the evolution of the $N = 82$ shell closure and its influence on the *r*-process nucleosynthesis. Such previously unreachable exotic nuclides have become accessible by means of in-flight fission of a high-intensity ^{238}U beam available at a new-generation radioactive isotope (RI) beam facility, the RI Beam Factory (RIBF) in RIKEN Nishina Center. In this report, recent spectroscopic results of Pd and Ag isotopes obtained as part of the EURICA (EUROBALL-RIKEN Cluster Array) project at RIBF are presented.

1 Introduction

The shell structures of atomic nuclei are nowadays known to change with the variation of the proton or neutron number, due predominantly to the monopole part of the proton-neutron interaction that includes the central and tensor forces [1]. Such a shell evolutionary behavior is expected to become pronounced when the proton-neutron imbalance is very large, leading to lost or new magic numbers [2]: For example, the conventional magic numbers $N = 8$, 20, and 28 disappear and new magicity emerges at $N = 16$, 32, and 34, depending on the location of the nucleus in the $N - Z$ plane. However, it is not known yet whether similar changes of the shell structure can take place at the heavier conventional magic numbers $N = 50$, 82, and 126, which also play an important role in determining the solar abundance distribution, particularly around the three prominent peaks at $A \approx 80$, 130, and 195, respectively, that would result from the rapid neutron-capture (*r*) process [3].

The advent of a new generation in-flight-separator facility, the RI-Beam Factory (RIBF) in RIKEN Nishina Center [4], has enabled us to explore previously inaccessible nuclear regions with a highly unbalanced ratio of neutrons to protons [5]. Neutron-rich palladium ($_{46}$Pd) isotopes, those with $A = 125 - 131$ ($N = 79 - 85$), have been identified as new isotopes at RIBF [6–8], followed by spectroscopic studies by means of β- and isomeric-decay measurements [9–11] and in-beam γ-ray spectroscopy [12] in the last decade. Especially emphasized is that delayed γ-ray measurements following isomeric decays can provide a powerful tool for investigating the excited level structure, in particular, when the nucleus of interest lies at the boundaries of availability for spectroscopic studies. For ^{128}Pd$_{82}$, which is a presumed waiting-point nucleus that contributes significantly to the formation of the second peak in the *r*-process solar abundance distribution [3, 13], a seniority isomer with a spin and parity of (8^+) had been identified, serving as indirect evidence for the robustness of the $N = 82$ shell closure [10]. In the two-neutron-hole neighbor ^{126}Pd$_{80}$, it turned out that the proton-neutron monopole properties of the central and tensor forces play an important role in the emergence of the long-lived (10^+) isomer [11]. Compared to such even-even systems, neighboring odd-mass nuclei exhibit more complicated excitation spectra, which provide crucial information on the effect of unpaired nucleons on the level structure. This proceedings reports on isomeric states and their decay properties in ^{125,127}Pd$_{79,81}$ [14] and low-lying β-emitting isomers in ^{123,125}Ag$_{76,78}$ [15].

2 Experimental details

Neutron-rich Pd and Ag isotopes were separated through the BigRIPS in-flight separator [16], following production via in-flight fission of a $^{238}U^{86+}$ beam at 345 MeV/u incident on a Be target with a thickness of 3 mm. The primary beam intensity ranged from 7 to 12 pnA during the experiments. The beamline included two wedge-shaped aluminum degraders with thicknesses of 2.9 and 2.5 mm at the first and second dispersive foci, respectively, and focal plane detectors such as position-sensitive parallel plate avalanche counters (PPACs), plastic scintillation counters, and ionization chambers. More detailed information on the detector configuration and the particle-identification analysis with the BigRIPS separator can be found in Ref. [17]. The ions of interest were transported through the BigRIPS-ZeroDegree spectrometer and finally implanted into the WAS3ABi active stopper, which consisted of eight layers of double-sided silicon-strip detectors (DSSSDs) stacked compactly [18]. Each DSSSD had

*e-mail: hiroshi@ribf.riken.jp

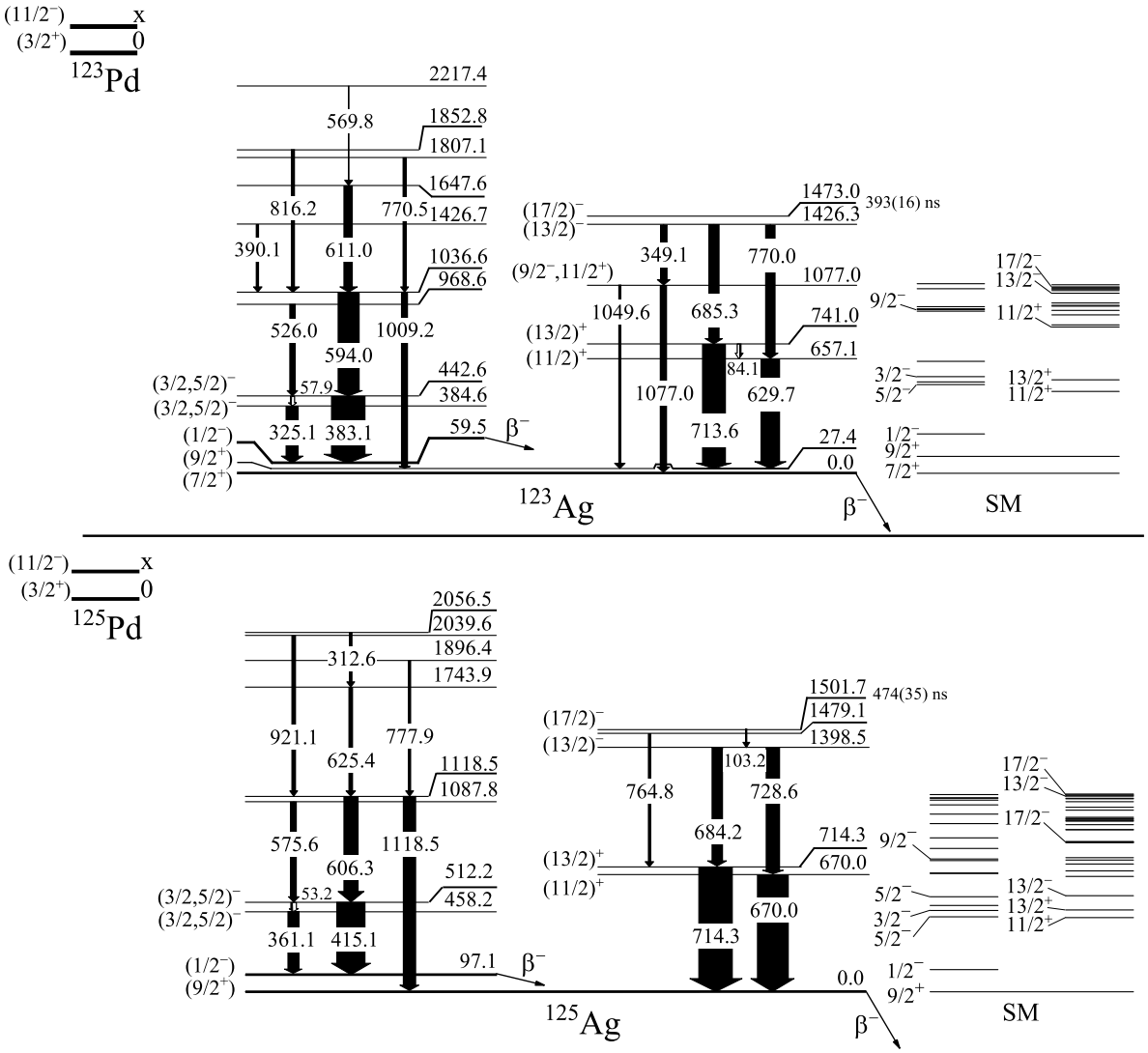

Figure 1. Partial level schemes of ^{123}Ag (upper) and ^{125}Ag (lower) presented in Ref. [15]. Levels predicted by shell-model (SM) calculations are shown on the right-hand side of each level scheme for comparison. Copyright (2019), with permission from the American Physical Society.

a thickness of 1 mm with an active area segmented into sixty and forty strips (1-mm pitch) on each side in the horizontal and vertical dimensions, respectively. Gamma rays emitted following the heavy-ion implantation and their subsequent radioactive decay were detected by the EURICA γ-ray spectrometer [18], consisting of 12 Cluster-type detectors, each of which contained seven HPGe crystals packed closely.

3 Results and discussions

3.1 ^{123}Ag$_{76}$ and ^{125}Ag$_{78}$

The excited states of ^{123}Ag and ^{125}Ag have been investigated following the β decays from the respective parent nuclei ^{123}Pd and ^{125}Pd. The decay schemes constructed in Ref. [15] are exhibited in Fig. 2. In addition to the previously reported transitions that are involved in the decay sequences from the $J^\pi = (17/2^-)$ isomeric states [19], a number of new γ rays have been observed in prompt coincidence with β rays. Note that the $(17/2^-)$ isomers were not clearly populated in the present work on account of the large spin difference from the parent levels. It turned out that there are two β-decaying states with similar half-lives in the parent Pd isotopes. Either a spin-parity of $11/2^-$ or $3/2^+$ is assigned for the β-decaying isomer, and the counterpart for the ground state. The β decay from the $11/2^-$ state is likely to feed $J = 9/2$, 11/2, and 13/2 levels in the daughter nucleus, while comparatively low-spin states can be populated in the β decay from the $3/2^+$ state. New results shown in Fig. 2 mainly include the transitions fed via the β decay from the $(3/2^+)$ states in ^{123}Pd and ^{125}Pd.

It can be seen that these two isotopes have a similar decay pattern. For ^{123}Ag, the 611-keV transition has a clear coincidence with the 1009-keV transition, as well as with the 383- and 594-keV transitions. Meanwhile, the 383- and 594-keV transitions are found to be in mutual coincidence, but not with the 1009-keV transition. The coinci-

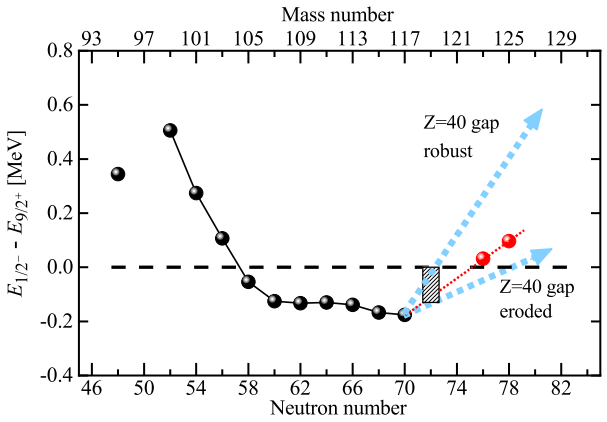

Figure 2. Systematics of experimental energy differences between the lowest-lying $1/2^-$ and $9/2^+$ states in odd-A Ag isotopic chain [15]. Copyright (2019), with permission from the American Physical Society.

dence pattern suggests that the 611-keV transition feeds a level, which decays via two parallel transition paths. Similarly, for ^{125}Ag, the 625-keV transition has a clear coincidence with the 1119-keV transition, as well as with the 415- and 606-keV transitions. Based on the γ-γ coincidences, intensity balance, and systematics of the odd-A Ag isotopes, for ^{125}Ag, the transition sequence of 415- and 606-keV is suggested to decay to the $(1/2^-)$ long-thought isomeric state, and the 1119-keV transition decays to the $(9/2^+)$ ground state. The remarkable similarity in γ-γ coincidence pattern in ^{123}Ag and ^{125}Ag suggests that, for ^{123}Ag, the transition sequence of 383- and 594-keV feeds the $(1/2^-)$ isomeric state, and the 1009-keV transition decays to the $(9/2^+)$ state.

Figure 2 exhibits the systematics of the measured energy difference between the lowest-lying $1/2^-$ and $9/2^+$ states in odd-A Ag isotopes as a function of the neutron number. These levels are interpreted as being ascribed to active proton holes in the $2p_{1/2}$ and $1g_{9/2}$ orbitals, respectively, which define a spherical sub-shell gap at $Z = 40$. The sizable (positive) energy difference around $N = 50$ indicates the stability of the $Z = 40$ gap. With increasing neutron number, this energy difference drops quickly. At $N = 58$, the ordering of these two levels swaps and the $1/2^-$ state becomes the lowest state. Following nearly flat evolution between $N = 58$ and 70, the order of these levels is inverted again at $N = 76$. However, the slope on the neutron-rich side is less steep than that on the neutron-deficient side, suggesting that the $Z = 40$ sub-shell gap is eroded when the neutron number increases towards $N = 82$.

3.2 ^{125}Pd$_{78}$ and ^{127}Pd$_{80}$

For ^{125}Pd, four γ rays at energies of 108, 115, 757, and 825 keV are clearly visible within a time interval of 250 – 1250 ns after the ion implantation, as exhibited in Fig. 3(a). They are unambiguously assigned as the transitions forming a single cascade from an isomeric state, which can be

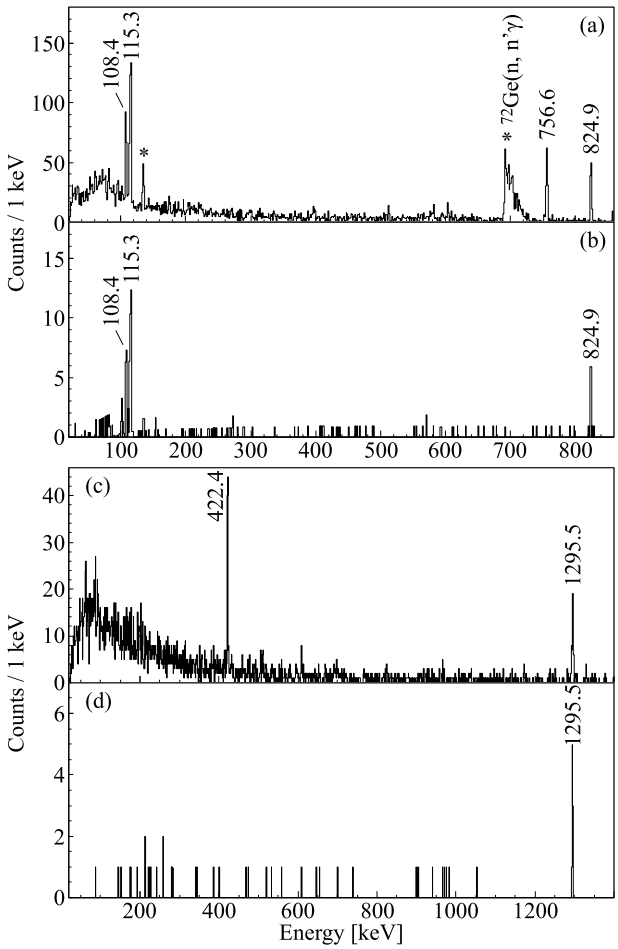

Figure 3. Gamma-ray energy spectra measured in Ref. [14]. The coincidence gate conditions are as follows. (a) and (b): Within a time range of 250 – 1250 ns after implantation of ^{125}Pd ions. Contaminants are marked with asterisks. An additional gate is set on the 757-keV γ ray to make the coincidence spectrum shown in the panel (b). (c) and (d): Within a time range of 0.25 – 100 μs after implantation of ^{127}Pd ions. An additional gate is set on the 422-keV γ ray to make the coincidence spectrum shown in the panel (c).

Table 1. Experimental and theoretical $B(\sigma\lambda)$ values for the selected transitions in ^{A}Pd isotopes.

			$B(\sigma\lambda)$ [W.u.]	
A	Transition	$\sigma\lambda$	Exp.	SM
125	$23/2^+ \rightarrow 19/2^+_2$	$E2$	3.47(9)	5.2
	$23/2^+ \rightarrow 19/2^+_1$	$E2$	-	1.1×10^{-7}
126	$7^- \rightarrow 5^-_2$	$E2$	2.13(14)	5.7
	$7^- \rightarrow 5^-_1$	$E2$	-	3.9×10^{-9}
127	$19/2^+ \rightarrow 15/2^-$	$M2$	$2.3(4) \times 10^{-3}$	7.6×10^{-3}

confirmed by their mutual coincidence as demonstrated in Fig. 3(b) and by their consistent time behavior. A weighted average of the respective fits to the decay curves results in an isomeric half-life of 144(4) ns. For ^{127}Pd, γ-ray peaks at 422 and 1296 keV have been prominently observed within a long time window ranging from 0.25 to 100 μs after the

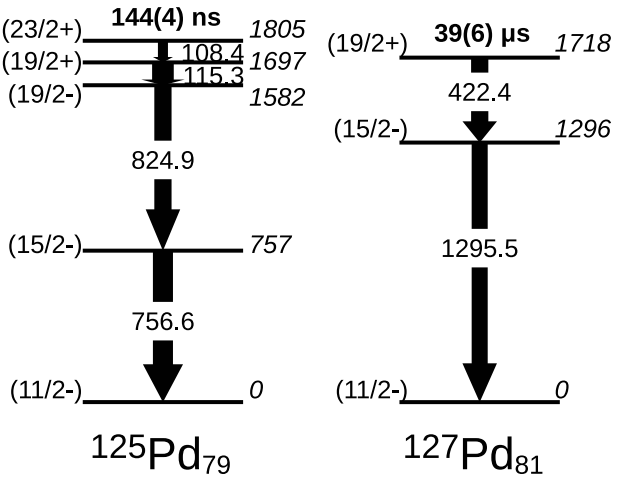

Figure 4. Level schemes of ^{125}Pd and ^{127}Pd established in Ref. [14]. Each level is labeled with the spin-parity (J^π) and energy (relative to the $11/2^-$ state) values. The measured (isomeric) half-lives are indicated in bold.

ion implantation, and their coincidence relationship confirmed by γ-γ coincidence analyses, see Figs. 3(c) and 3(d). The isomeric half-life was determined to be 39(6) μs from a weighted average of the respective fits to the time distributions of the 422- and 1296-keV γ rays. The level schemes of ^{125}Pd and ^{127}Pd are shown in Fig. 4. More detailed arguments on the spin-parity assignments are given in Ref. [14].

To interpret systematically the level properties of the neutron-rich Pd isotopes towards $N = 82$, shell-model calculations based on the extended pairing plus quadrupole-quadrupole forces combined with monopole corrections (EPQQM) [20] have been performed for ^{125,126,127,128}Pd. With the doubly magic nucleus ^{78}Ni as the closed core, the model space considered includes four orbits in the $Z = 28 - 50$ major shell and the $g_{7/2}$, $d_{5/2}$ orbits above the $Z = 50$ shell gap for protons, and five orbits in the $N = 50 - 82$ major shell and the $f_{7/2}$, $p_{3/2}$ orbits above the $N = 82$ shell gap for neutrons. The observed and calculated level energies are compared in Fig. 5, where the columns marked with SM exhibit the results of a large-scale shell model that allows the excitation of a neutron across the shell gap of $N = 82$. The measured and calculated values of the reduced transition probabilities for the selected transitions are summarized in Table 1.

For the higher-lying levels in ^{125}Pd, the shell-model calculation predicts that there are two $19/2^+$ states below an excitation energy of 2 MeV, as indicated with different colors in Fig. 5. The $19/2^+_1$ state is predicted to involve predominantly a two-proton-hole excitation $\pi(g^{-1}_{9/2}p^{-1}_{1/2})$ together with an inactive proton-hole pair $\pi(g^{-2}_{9/2})_{0^+}$, coupled to an active neutron hole in the $h_{11/2}$ orbit (and a neutron-hole pair coupled to spin zero). Meanwhile, the $19/2^+_2$ state is dominated by neutron-hole excitations of the type $(\nu^{-3})_{19/2^+}$, such as $\nu(h^{-2}_{11/2}d^{-1}_{3/2})$, $\nu(h^{-2}_{11/2}s^{-1}_{1/2})$, and $\nu(h^{-2}_{11/2}g^{-1}_{7/2})$, coupled to an inactive proton component, $\pi(g^{-4}_{9/2})_{0^+}$ or $\pi(g^{-2}_{9/2}p^{-2}_{1/2})_{0^+}$. Thus, the proton and neutron excitations within the respective major shells are suggested to compete with each other in ^{125}Pd.

According to the present shell-model calculation for ^{125}Pd, the major components of the $23/2^+$ wave function differ significantly from those of the $19/2^+_1$ state, resulting in a strongly hindered $E2$ transition (see Table 1). On the other hand, very similar wave functions are predicted for the $23/2^+$ and $19/2^+_2$ states of ^{125}Pd. The fact that the measured $B(E2)$ value for the isomeric deexcitation is fairly consistent with the calculated $B(E2; 23/2^+ \rightarrow 19/2^+_2)$ value indicates that both the experimental $(23/2^+)$ and $(19/2^+)$ levels are dominated by the neutron excitations. A candidate for the $19/2^+_1$ shell-model state, which is dominated by the proton excitations, has not been identified in the current experiment.

Similar decay patterns are suggested to take place in the one-neutron neighbor ^{126}Pd. As compared in Table 1, the experimental $B(E2)$ value for the $(7^-) \rightarrow (5^-)$ transition [10] is well reproduced by SM given the $E2$ transition towards the 5^-_2 level, thus suggesting that the calculated 5^-_2 level corresponds to the (5^-) state observed at 2023 keV [10]. In contrast, the $7^- \rightarrow 5^-_1$ deexcitation is calculated to be extremely hindered, similar to the aforementioned $23/2^+ \rightarrow 19/2^+_1$ transition in ^{125}Pd. Analyzing the shell-model wave functions, it can be found that the main configurations of the $5^-_{1,2}$ and 7^- states in ^{126}Pd are almost equivalent to the $19/2^+_{1,2}$ and $23/2^+$ states in ^{125}Pd, respectively, with the addition of a neutron in the $h_{11/2}$ orbit, i.e., the proton excitations and neutron excitations, respectively, dominate the 5^-_1 level and the 5^-_2, 7^- levels.

The excitation spectra and the reduced transition probability for the $(19/2^+) \rightarrow (15/2^-)$, $M2$ decay observed for ^{127}Pd are reproduced satisfactorily by the shell-model calculation. The $19/2^+$ state is predicted to have a wave function with the leading component, $\pi(g^{-3}_{9/2}p^{-1}_{1/2})\otimes\nu(h^{-1}_{11/2})$, the analog of the $19/2^+_1$ state in ^{125}Pd. The wave function of the $15/2^-$ state, to which the $19/2^+$ isomer decays, consists predominantly of the $\pi(g^{-4}_{9/2}) \otimes \nu(h^{-1}_{11/2})$ component. Hence, an $M2$ decay cannot proceed between their main configurations. Within the $Z = 28 - 50$ major shell, an $M2$ decay can take place through the $\pi f_{5/2} \rightarrow \pi g_{9/2}$ transition. It is, therefore, expected that the large hindrance of the order of 10^{-3} W.u. (see Table 1) is ascribed to the small admixture of the $\pi(g^{-3}_{9/2}f^{-1}_{5/2}) \otimes \nu(h^{-1}_{11/2})$ component in the $19/2^+$ isomeric state.

Finally, it is noteworthy that for the $N = 82$ closed-shell nucleus ^{128}Pd an excited state with a spin and parity of 5^- is predicted to be lower in energy than both the experimental and theoretical 4^+ levels, as shown in Fig. 5. The main component of the 5^- state is $\pi(g^{-3}_{9/2}p^{-1}_{1/2})$, the same as that involved in the $19/2^+$ state of ^{127}Pd, which is well reproduced by the present shell-model calculations, as discussed in the last paragraph. With the calculated energies and $B(E3; 5^- \rightarrow 2^+)$, as well as the theoretical α_T value [21], the half-life of the 5^- state is estimated to be 5 ms. Such a long-lived isomer has not been identified in Refs. [10, 11] due presumably to insufficient statistics,

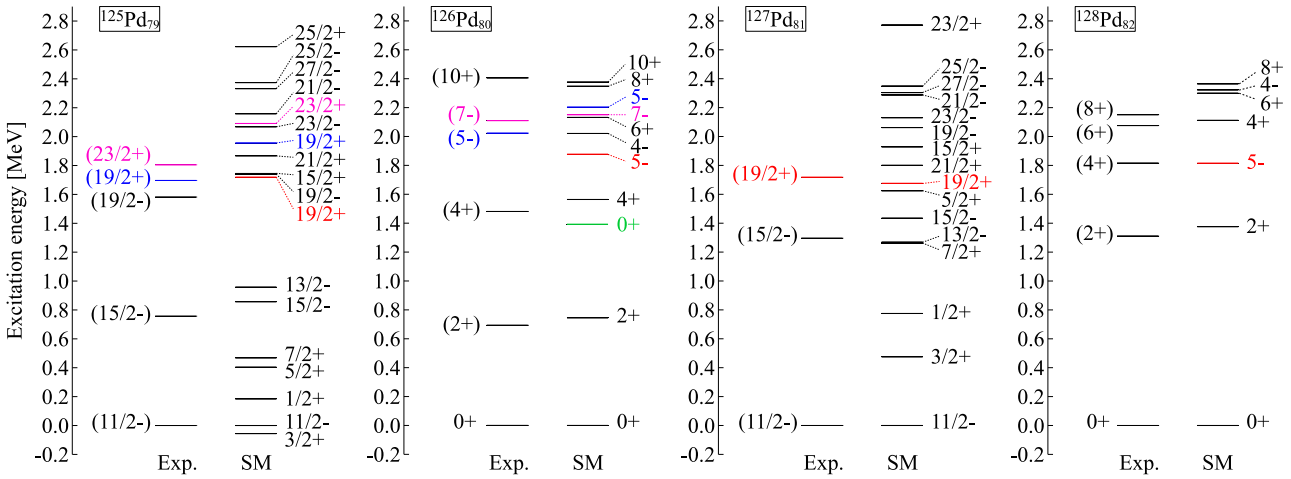

Figure 5. Comparison between experimental and shell-model (SM) level energies in ^{125,126,127,128}Pd isotopes.

remaining a challenge for future experiments using more intense radioactive-isotope beams.

References

[1] T. Otsuka, Y. Tsunoda, J. Phys. G Nucl. Partic. **43**, 024009 (2016).
[2] O. Sorlin, M. G. Porquet, Prog. Part. Nucl. Phys. **61**, 602 (2008).
[3] E. M. Burbidge, G. R. Burbidge, W. A. Fowler, F. Hoyle, Rev. Mod. Phys. **29**, 547 (1957).
[4] Y. Yano, Nucl. Instrum. Meth. B **261**, 1009 (2007).
[5] T. Nakamura, H. Sakurai, H. Watanabe, Prog. Part. Nucl. Phys. **97**, 53 (2017).
[6] T. Ohnishi, T. Kubo, K. Kusaka *et al.*, J. Phys. Soc. Jpn. **77**, 083201 (2008).
[7] T. Ohnishi, T. Kubo, K. Kusaka *et al.*, J. Phys. Soc. Jpn. **79**, 073201 (2010).
[8] Y. Shimizu, T. Kubo, N. Fukuda *et al.*, J. Phys. Soc. Jpn. **87**, 014203 (2018).
[9] G. Lorusso, S. Nishimura, Z.Y. Xu *et al.*, Phys. Rev. Lett. **114**, 192501 (2015).
[10] H. Watanabe, G. Lorusso, S. Nishimura *et al.*, Phys. Rev. Lett. **111**, 152501 (2013).
[11] H. Watanabe, G. Lorusso, S. Nishimura *et al.*, Phys. Rev. Lett. **113**, 042502 (2014).
[12] H. Wang, N. Aoi, S. Takeuchi *et al.*, Phys. Rev. C **88**, 054318 (2013).
[13] K. L. Kratz, B. Pfeiffer, O. Arndt *et al.*, Eur. Phys. J. A **25**, 633 (2005).
[14] H. Watanabe, H. Wang, G. Lorusso *et al.*, Phys. Lett. B **792**, 263 (2019).
[15] Z. Q. Chen, Z. H. Li, H. Hua *et al.*, Phys. Rev. Lett. **122**, 212502 (2019).
[16] T. Kubo, D. Kameda, H. Suzuki *et al.*, Prog. Theor. Exp. Phys. **2012**, 03C003 (2012).
[17] N. Fukuda, T. Kubo, T. Ohnishi *et al.*, Nucl. Instrum. Meth. B **317**, 323 (2013).
[18] S. Nishimura, Prog. Theor. Exp. Phys. **2012**, 03C006 (2012).
[19] S. Lalkovski, A. M. Bruce, A. Jungclaus *et al.*, Phys. Rev. C **87**, 034308 (2013).
[20] M. Hasegawa, K. Kaneko, Phys. Rev. C **59**, 1449 (1999).
[21] T. Kibédi, T. W. Burrows, M. B. Trzhaskovskaya *et al.*, Nucl. Instrum. Meth. A **589**, 202 (2008).